A dedicated ML-algorithm for non-attenuation corrected PET whole body images. [1]

J. Nuyts, S. Stroobants, P. Dupont, S. Vleugels, P. Flamen, L. Mortelmans
Nuclear Medicine, K.U.Leuven, B3000 Leuven, Belgium

keywords: PET, attenuation correction, iterative reconstruction, contrast, tumor to background ratio.

Correspondence and reprints: Johan Nuyts
Dept. of Nuclear Medicine
University Hospital Gasthuisberg
Herestraat 49
3000 Leuven
Belgium
Tel: (32) 16.34.37.15
Fax: (32) 16.34.37.59

Abstract

In whole body positron emission tomography, it is common practice to omit the transmission scan to shorten the study time. Consequently, the emission sinograms are reconstructed without attenuation correction. Although this leads to artifacts in the reconstructed images, it has been shown that these images still provide valuable diagnostic information in oncological applications. Analysis of the attenuation artifact reveals that it consists of two components: a multiplicative and an additive component. The presence of the additive component explains why tumor to background ratio decreases with attenuation correction, a puzzling finding reported by several groups. In cases of strong attenuation, the negative additive component can have an adverse effect on image quality in maximum-likelihood reconstruction. The problem is caused by the non-negativity constraint of that algorithm. We propose a new ML-algorithm in which this constraint is removed to preserve image quality. Since the introduction in the clinical routine in our department, the algorithm has been applied to over 2000 studies with satisfactory results.

[1]This work is supported by the Flemish Fund for Scientific Research (FWO), grant number G.0106.98. P. Dupont is post-doctoral researcher of the FWO.

I. Introduction

Positron emission tomography (PET) with fluorodeoxyglucose is being used increasingly in oncological applications. Often a PET scan is acquired over a large part of the body, aiming at detection of possible unknown metastases. Currently, these so-called whole body studies are often done without transmission scan and the images are reconstructed without attenuation correction. Until recently, the transmission scan had to be done prior to injection, while the emission scan was only acquired about an hour after injection, so the transmission scan would increase the total study time with more than an hour. Recently, post-injection transmission scanning allows to correct for attenuation with only a moderate increase of scanning time. However, the effect on visual image quality is controversial [1, 2], and many clinical centers still prefer the protocol without transmission scanning.

II. Theory

Consider a infinitely thin ring of activity concentrically embedded in an otherwise cold attenuating disk. The attenuated projection acquired along a line with angle θ at a distance x from the origin equals

$$\begin{aligned} I(x,\theta) &= e^{-2\mu\sqrt{R_A^2-x^2}}\frac{2\lambda R}{\sqrt{R^2-x^2}} \text{ for } |x| \le R \quad (1)\\ &= 0 \text{ for } |x| > R \end{aligned}$$

where R is the radius of the ring, $R_A > R$ is the radius of the attenuating disk, λ is the radioactivity per unit length in the ring and μ is the linear attenuation coefficient.

The sinogram $I(x,\theta)$ is symmetrical and independent of the angle. Consequently, it is consistent under the assumption of zero attenuation [3], and an exact solution exists. An integral expression of this solution can be obtained by direct application of filtered backprojection, or by applying an operator which computes the point spread function from the line spread function [4]. Solving this integral is cumbersome, but important features of the solution can be easily derived mathematically or numerically. In appendix A, we show mathematically that the solution is negative everywhere within the radioactive ring. Since an exact solution exists, a good estimate can be obtained numerically with a discrete filtered backprojection (FBP) program. The profile in figure 1 clearly shows that central pixel values are reconstructed with negative values. Since the superposition principle holds, it follows that reconstructed pixel values receive a negative contribution which increases with increasing amounts of surrounding activity.

A. Contrast

It is well known that lack of attenuation correction results in a severe underestimation of true activity, because a fraction of the photons emitted towards the detector has been eliminated by attenuation. As shown above, a more subtle attenuation artifact results in negative additive contributions from surrounding activity. This negative additive component

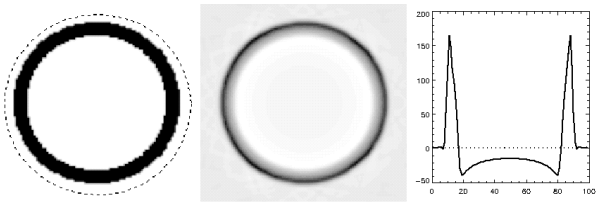

Figure 1: Left: original activity distribution, dotted line indicates attenuating disk. Center: reconstruction without attenuation correction from attenuated projections. Right: profile through the center of the reconstruction image.

is the reason that ignoring attenuation correction tends to increased tumor to background ratios, as has been reported by several investigators [1, 5, 6]. Assuming tumor activity T and background activity B, and assuming that the effect of the attenuation artifact can be described with regionally constant multiplicative and additive components m and a, reconstruction without attenuation correction would result in an apparent ratio R of

$$R = \frac{mT-a}{mB-a} > \frac{T}{B} \text{ , if } T > B. \quad (2)$$

The additive component behaves as a "background subtraction", increasing the contrast. There is no indication that this effect would also suppress noise, so the increased contrast does not imply improved signal to noise ratio or improved tumor detection.

B. Negative values

In large patients, the negative additive component of the attenuation artifact can make entire regions negative. However, these regions may still contain useful visual information, superimposed on the negative additive component of the artifact. In clinical applications, FBP often produces negative pixel values in regions where attenuation was important. However, FBP is very sensitive to noise and tends to produce disturbing streak artifacts. In contrast, the maximum-likelihood expectation-maximization (MLEM) is more robust against noise, but has a built-in non-negativity constraint. When used with attenuation correction this is an obvious strength, but if no attenuation correction is included the constraint becomes a weakness, and highly attenuated regions are reconstructed as uniform regions with (nearly) zero tracer uptake. As a result, useful image detail may be lost.

III. The dedicated ML-algorithm

The MLEM algorithm [7] can be regarded as a scaled gradient ascent algorithm, where the step size is scaled such that it prevents negative values. In appendix B an alternative step size is derived, allowing the inclusion of negative values while preserving the desirable features of the MLEM-algorithm. The new algorithm is a successful heuristic approach to obtain good visual image quality but obviously lacks theoretical justification in physics, since negative activities are meaningless.

After a pilot study, the new algorithm has been introduced in

clinical routine and has been applied to over 2000 PET whole body studies. The physicians accept it as a good compromise between FBP and MLEM, and use it both for diagnosis and for documentation. Figure 2 compares a coronal view obtained with the three reconstruction algorithms.

IV. Conclusion

A new dedicated ML-algorithm for the reconstruction of whole body images without attenuation correction is proposed. It has been introduced in clinical practice with good results.

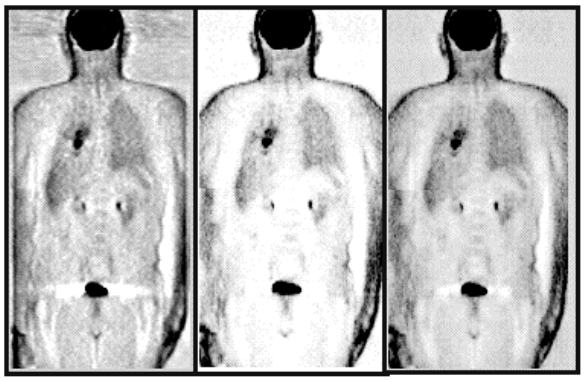

Figure 2: Left: FBP reconstruction. Center: MLEM reconstruction. Right: modified MLEM reconstruction.

V. Appendix A

Since all projections are identical, the reconstruction of (1) is radially symmetrical and can be represented as $f(x^2+y^2) = f(z)$. The projection can be regarded as a line spread function, the reconstruction as the corresponding point spread function. The solution is given by [4]:

$$f(z) = \frac{-2}{\pi}\frac{d}{dz}\int_0^\infty A(v^2+z)dv \qquad (3)$$

with $A(x^2) = I(x,\theta)$. Inserting (1) produces

$$f(z) = \frac{-4\lambda R}{\pi}\frac{d}{dz}\int_0^{\sqrt{R^2-z}} \frac{e^{-2\mu\sqrt{R_A^2-v^2-z}}}{\sqrt{R^2-v^2-z}}dv. \qquad (4)$$

Substituting $\omega = v/\sqrt{R^2-z}$ and taking the derivative under the integral sign results in

$$f(z) = \frac{-4\lambda R\mu}{\pi}\int_0^1 \frac{e^{-2\mu\sqrt{R_A^2-z-\omega^2(R^2-z)}}\sqrt{1-\omega^2}}{\sqrt{R_A^2-z-\omega^2(R^2-z)}}d\omega \qquad (5)$$

which is negative for $z < R^2$ and $\mu > 0$.

VI. Appendix B

The likelihood for emission tomography can be written as

$$\sum_i h_i(r_i) = \sum_i (y_i \ln r_i - r_i) \text{ with } r_i = \sum_j c_{ij}\lambda_j \qquad (6)$$

where y_i is the measured count in detector i, λ_j is the (unknown) activity in pixel j and c_{ij} is the assumed detection probability (ignoring attenuation). A surrogate function [8, 9] is introduced to separate the variables (the prime denotes current reconstruction value):

$$\sum_i h_i(r_i) = \sum_i h_i\left(\sum_j \pi_{ij}\left(\frac{c_{ij}}{\pi_{ij}}(\lambda_j-\lambda_j')+r_i'\right)\right) \qquad (7)$$

$$\geq \sum_i\sum_j \pi_{ij} h_i\left(\frac{c_{ij}}{\pi_{ij}}(\lambda_j-\lambda_j')+r_i'\right), \qquad (8)$$

with equality if $\lambda_j = \lambda_j'$. The constants π_{ij} must satisfy $\sum_j \pi_{ij} = 1$ but are otherwise arbitrary. Equation (8) follows from the concavity of h_i. Consequently, maximizing (8) yields an increase of the likelihood (7), unless both have reached their maximum. Applying Newton's method to each term of (8), replacing y_i/r_i^2 with $1/y_i$ in the denominator and choosing $\pi_{ij} = c_{ij}/\sum_k c_{ik}$ yields:

$$\lambda_j = \lambda_j' + \left[\frac{1}{\sum_i \frac{c_{ij}}{y_i}\sum_k c_{ik}}\right]\sum_i c_{ij}\frac{y_i - r_i'}{r_i'}. \qquad (9)$$

The factor between squared brackets is the step size, which does not vanish when λ_j approaches zero. This algorithm turns out to be conservative; we compute also the MLEM step size in every pixel and apply the larger of the two.

VII. References

[1] M Lonneux, I. Borbath et al. "Attenuation correction in whole-body FDG oncological studies: the role of statistical reconstruction." *Eur J Nucl Med*, vol 26; pp 591-598, 1999.

[2] TH Farquhar, J Llacer et al. "ROC and localization ROC analyses of lesion detection in whole-body FDG PET: effects of acquisition mode, attenuation correction and reconstruction algorithm", *J Nucl Med*, vol 40; pp 2043-2052, 1999.

[3] F Natterer. "Determination of tissue attenuation in emission tomography of optically dense media." *Inverse problems*, vol 9, pp 731-736, 1993.

[4] EW Marchand. "Derivation of the point spread function from the line spread function", *J Opt Soc Am*, vol 54, pp 915-919, 1964.

[5] M.B. Imran, K. Kubota et al. "Lesion-to-background ratio in nonattenuation corrected whole-body FDG PET images." *J. Nucl. Med., vol. 39*, pp 1219-1223, 1998.

[6] F.M. Bengel, S.I. Ziegler et al. "Whole-body positron emission tomography in clinical oncology: comparison between attenuation-corrected and uncorrected images." *Eur. J. Nucl. Med., vol. 24*, pp 1091-1098, 1997.

[7] L Kaufman. "Maximum likelihood, least squares and penalized least squares for PET." *IEEE Trans Med Imaging*, vol 12, pp 200-214, 1993.

[8] AR De Pierro. "A modified expectation maximization algorithm for penalized likelihood estimation in emission tomography," *IEEE Trans Med Imaging*, vol 14, pp 132-137, 1995.

[9] JA Fessler, EP Ficaro et al. "Grouped-coordinate ascent algorithms for penalized-likelihood transmission image reconstruction," *IEEE Trans Med Imaging*, vol 16, pp 166-175, 1997.